Journal of Rheology

RESEARCH ARTICLE | JULY 01 2022

Understanding the complex rheology of human blood plasma

T. Rodrigues ; R. Mota ; L. Gales ; L. Campo-Deaño

J. Rheol. 66, 761–774 (2022)
https://doi.org/10.1122/8.0000442

Understanding the complex rheology of human blood plasma

T. Rodrigues,[1,2] R. Mota,[3,4] L. Gales,[3,4,5] and L. Campo-Deaño[1,2,a)]

[1]*CEFT—Centro de Estudos de Fenómenos de Transporte, Depto. de Engenharia Mecânica, Faculdade de Engenharia, Universidade do Porto, Rua Dr. Roberto Frias, 4200-465 Porto, Portugal*
[2]*ALiCE—Laboratório Associado em Engenharia Química, Faculdade de Engenharia, Universidade do Porto, Rua Dr. Roberto Frias, 4200-465 Porto, Portugal*
[3]*i3S—Instituto de Investigação e Inovação em Saúde, Universidade do Porto, Rua Alfredo Allen, 208, 4200-135 Porto, Portugal*
[4]*IBMC—Instituto de Biologia Molecular e Celular, Universidade do Porto, Rua Alfredo Allen, 208, 4200-135 Porto, Portugal*
[5]*ICBAS—Instituto de Ciências Biomédicas Abel Salazar, Universidade do Porto, Rua de Jorge Viterbo Ferreira, 228, 4050-313 Porto, Portugal*

(Received 16 January 2022; final revision received 2 May 2022; published 15 June 2022)

Abstract

Blood plasma (BP) is a borderline non-Newtonian fluid. Few studies have characterized the rheology of BP and even less focused on understanding its subtle viscoelastic traits, which were only somewhat recently acknowledged. We use passive microrheology to measure the bulk response of human plasma samples under shear at body and ambient temperatures. Evidence of subdiffusive behavior in the mean-squared displacement is observed at the highest frequencies probed, which we attribute to the stress relaxation of protein molecules or chains. Jeffreys-like complex shear moduli were computed thereof. The microenvironments of albumin, fibrinogen, and gamma-globulin solutions (key plasma proteins) were probed as well. Single proteins in an aqueous buffer showed no signs of viscoelasticity within experimental resolution. Conversely, mixed together, they appear to promote the same kind of short-term elastic behavior seen in plasma. All in all, a fresh look at the shear rheology of BP is presented. https://doi.org/10.1122/8.0000442

I. INTRODUCTION

The blood that runs inside our veins is a viscoelastic fluid. Numerous studies devoted to characterizing, modeling, and understanding its non-Newtonian behavior enrich the literature that we know of today [1–4]. On the surface, blood exhibits a shear-thinning response under steady shear and some bulk elasticity—with a longest extensional relaxation time (λ) of 2–3 ms [5]. Less obvious and equally contributing to its complex nature are other features, including but not limited to thixotropy. Not as investigated as whole blood, however, is plasma, the solvent in which all of the former's cellular elements are suspended: red blood cells (RBCs), white blood cells (WBCs), and platelets. Blood plasma (BP) accounts for over half of the blood's volume, and the better part of it is plain water (Fig. 1). In addition to water, BP is a mixture of proteins, electrolytes, carbohydrates, and lipids (roughly 8% by volume). Its protein composition is rather diverse (Table I), albeit albumin, globulins, and fibrinogen are commonly mentioned. While albumin is the most abundant, globulins comprise proteins such as antibodies, i.e., immunoglobulins; lastly, fibrinogen is the protein that promotes the final push toward blood's coagulation, despite its low concentration in plasma [6].

Interestingly, BP is, too, viscoelastic, albeit having been regarded as Newtonian until recently. The weakly elastic behavior of the biofluid was possibly first reported by Brust *et al.* [5], who measured its λ under uniaxial extensional flow using a CaBER-like[1] apparatus (which is, in essence, a technique for tensile testing on fluids). They determined the longest relaxation times of 0.9 and 0.5 ms at 20 and 37 °C (core body temperature), respectively; not far from those of whole blood. Moreover, the flow of BP was investigated through a microfluidic contraction–expansion in order to assess the combined effects of shear (near the walls) and extensional (along the centerline) fluid deformations on the pressure drop as a function of flow rate. They observed a non-Newtonian response here as well, in the form of a nonlinear profile (which would otherwise be linear for a Newtonian liquid). Ultimately, the viscoelasticity of BP can only be attributed to macromolecular relaxations. Much like polymers, shear and extension may cause proteins to denature and stretch (also rotate), returning afterward to their initial conformational state (taking a given relaxation time to do so). Plasma proteins and their elongational properties also have a say in the bulk flow behavior of whole blood, either through direct (the viscoelasticity

a)Author to whom correspondence should be addressed; electronic mail: campo@fe.up.pt

[1]Capillary breakup extensional rheometer (CaBER).

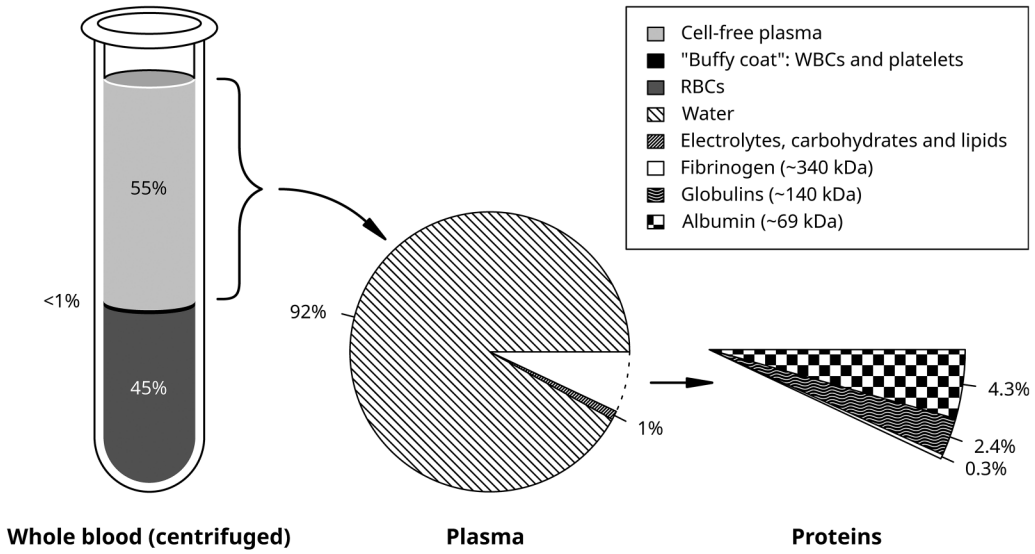

FIG. 1. Average composition of blood (after centrifugation) and plasma [7].

of the biological solvent) or indirect (by promoting RBC aggregation) [8] influence.[2]

More recently, Varchanis *et al.* [9] and Sousa *et al.* [2] revisited the subject using numerical and experimental approaches, respectively. The former presented a comprehensive study of the rheology of BP based on thorough numerical modeling, using an optimization procedure for fine-tuning a multimode Giesekus fluid model to match its linear and nonlinear behavior under selected flows. The simulations were successful in estimating novel material functions from the experimental data gathered by Brust *et al.* [5]. However, limited rheological information concerning the linear viscoelasticity of the biofluid was available at the time, mostly due to the mechanical limitations of modern rheometers, which lack the sensitivity required for such measurements. Recent small amplitude oscillatory shear (SAOS) tests with platelet-rich BP (considerably more viscoelastic than bare plasma) by Mitra and co-workers are a good example of just how difficult, not to say impossible, it is to extract reliable data from low viscosity weakly elastic fluids via conventional bulk shear rheometry [10]. Even Horner *et al.* [1] who characterized the rheology of whole blood struggled with its also weak inner structure, having conducted most of the oscillatory tests outside the linear region of small deformations for that reason. Hence, the elastic behavior of BP under shear (i.e., its elastic modulus G') is still a matter of debate, except for the first-ever numerical prediction to include a spectrum of relaxation times (presented in the aforementioned work) [9] and the recent evidence of a solidlike response using a custom parallel disk (PD) fixture that promotes wetting [11]. Sousa *et al.* [2] also used a custom-made CaBER-like setup to measure the λ of BP and whole blood. They reported relaxation times of almost an order of magnitude shorter than those measured by Brust *et al.* [5], which was attributed to possible differences between the two plasma collection protocols, e.g., the ratio and type of anticoagulant used in the blood samples.[3]

Herein, we take a fresh look at the shear rheology of not only BP but also its main proteins [bovine serum albumin (BSA), fibrinogen (Fg), and gamma-globulins (γ-g); highlighted in Table I] in solution at physiological concentrations. Since this biofluid is, in essence, a dilute protein solution, its biomacromolecular composition, structure, and respective reptation (relaxation) dynamics determine the strain response of the bulk under an applied stress. Like polymer chains or DNA [12], proteins in general can, too, influence how the solutions in which these are dissolved flow. Despite the long-standing interest in plasma proteins—mainly oriented toward understanding the biophysical properties of whole blood—little is still known about their contribution to overall BP rheology [2,9]. We demonstrate that multiple particle tracking (MPT) microrheology enables measurements of network viscoelasticity in human plasma. This passive microrheological technique has been widely employed to quantify the mechanical properties of complex biomaterials [13,14,63] and protein solutions [15–19] in the low moduli range, without bulk strain and requiring only minute sample volumes. Further, we show that mixtures of the plasma proteins investigated exhibit the same type of Jeffreys-like fluid rheology as BP, whereas the single protein solutions behaved as purely viscous within experimental resolution. We discuss these results in terms of possible protein dynamics that promote the viscoelasticity of the internal molecular matrix the likes of other weakly elastic protein systems that display similar non-Newtonian behavior [13,16].

[2]RBCs aggregate into rouleaux not only in periods of stasis but also at high shear rates, as a consequence of BP proteins such as fibrinogen. Some of these aggregates (reversibly) break apart as a result of fluid stresses and single RBCs are capable of elongation as well, granting the biofluid its main non-Newtonian features.

[3]Were it serum instead of plasma (minding the different rheology), the addition of anticoagulant to whole blood would not matter since the former—being deprived of fibrinogen—cannot clot.

TABLE I. Major plasma proteins (normal concentration range of total protein is 60–80 mg ml^{-1}) [6]. Low-density lipoprotein (LDL).

Protein fractions of human plasma				Molecular weight (kDa)	Concentration (mg ml^{-1})
Transthyretin				62	<1.5
Albumin				69	35–55
Globulins	α_1	α_1-Antitrypsin (α_1AT)		54	1–4
		⋮			
	α_2	α_2-Macroglobulin		725	4–11
		Haptoglobin		100	
		⋮			
	β	β-Lipoprotein (LDL)		380	5–12
		Transferrin		80	
		⋮			
	γ	**Immunoglobulins (Ig)**	IgA	160	7–17
			IgD	170	
			IgE	190	
			IgG[a]	150	
			IgM	970	
		⋮			
Complement C3				185	<1.5
Fibrinogen				340	1.5–3
⋮					

[a]About 75% of Ig.

II. MATERIALS AND METHODS

A. Plasma samples and protein solutions

Aliquots of BP collected from three healthy subjects (samples #1, #2, and #3) were stored at −80 °C in Falcon tubes. The platelet-free plasma (kindly provided by Hospital de Santo António, Porto, Portugal) was obtained by centrifuging the blood samples after withdrawal. Prior to use, each human plasma sample was thawed to roughly 4 °C overnight. The relevant physical and rheological properties of the biofluid are shown in Table II.

Proteins were chosen based on their molecular weight and concentration in normal plasma (see Table I). All the proteins were obtained from Sigma-Aldrich and dissolved in a physiological phosphate-buffered saline (PBS) formulated in-house (0.02 M sodium phosphate, 0.154 M NaCl, *p*H 7.4) to a final volume of 1 ml each, with the exception of human immunoglobulin M (IgM), which was already provided as a solution in a Tris-buffered saline (TBS) and was used as received. Target concentrations (c_{tar}) were those at which the proteins are typically found in normal BP (Table III). In addition to the single protein solutions, mixtures M1 (BSA + Fg + IgG) and M2 (BSA + Fg + γ-g) were prepared from the initial working stocks—ensuring the same individual effective concentrations (c_{eff}) as before. Following dissolution, all preparations were refrigerated (at about 4 °C) and used for experiments within 12 h. The structures of the main plasma proteins investigated herein are shown in Fig. 2.

TABLE II. Selected properties of human blood plasma at reference and body temperatures. From left to right: density (measured using pycnometer), and zero- (extracted from MSD) and plateau (bulk rheology measurement) shear viscosities. Uncertainties are given as two-sigma errors of the means ($\bar{X} \pm 2\sigma$).

	ρ (g ml^{-1})	η_0^{BP} (mPa s)	η_∞ (mPa s)
20 °C	1.027 ± 0.001[b]	1.82 ± 0.06[a]	1.67 ± 0.01[b]
37 °C	n/a	1.27 ± 0.02[b]	1.23 ± 0.01[b]

[a]Averaged across all samples.
[b]Sample #3 (more volume available).

B. Multiple particle tracking microrheology

MPT microrheology was used to measure the rheological properties of the human BP samples and protein solutions. MPT is a passive microrheological technique in which the Brownian motion of probe particles is measured and related

TABLE III. Single plasma protein solutions probed. Product number and details, effective and target concentrations, and *p*H in solution.

	Product no.	Origin	Form	c_{eff} (c_{tar}) (mg ml^{-1})	*p*H
BSA	A7906	Bovine	Powder	44.8 (45)[a]	7.4[c]
Fg	F3879	Human		2.8 (2.5)[a]	
IgG	I4506	Human		13.0 (12)[a]	
γ-g	G5009	Bovine		16.0 (16)[a]	
IgM	I8260	Human	TBS	0.8–1.2 (1)[b]	8.0

[a]Quantification using NanoDrop spectrophotometer (A280 measurement).
[b]Effective range specified by the supplier (A280 measurement).
[c]PBS.

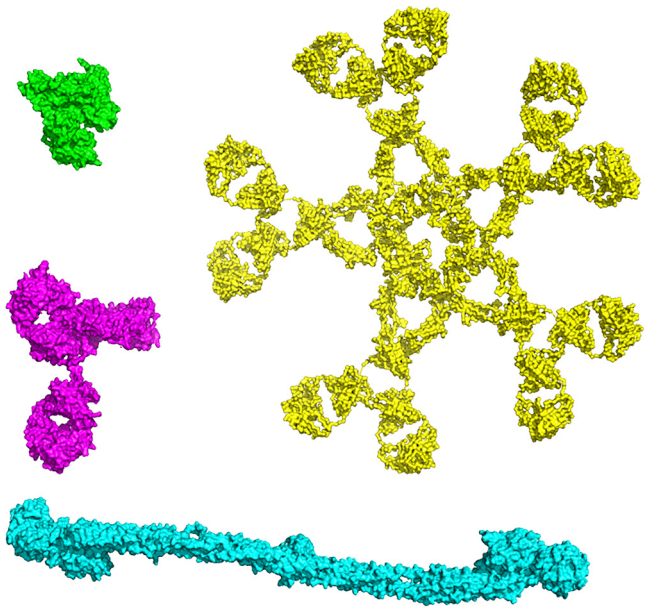

FIG. 2. Structures of BSA (upper left, or green in online figure), IgG (left center, or purple in online figure), Fg (bottom, or blue in online figure), and pentameric IgM (upper right, or yellow in online figure) to scale. Atomic models obtained from the protein data bank (PDB) with IDs: 4F5S [20], 1HZH [21], 3GHG [22], and 2RCJ [23], respectively. The length of the Fg molecule is 4.5 nm (45 Å).

to bulk rheological properties using the generalized Stokes–Einstein relation (GSER) by

$$J(\tau) = \frac{3\pi a}{dk_B T}\left\langle \Delta r^2(\tau)\right\rangle, \tag{1}$$

where J is the creep compliance, τ is the lag time, $k_B T$ is the thermal energy, d is the number of spatial dimensions, a is the probe radius and $\langle \Delta r^2 \rangle$ is the two-dimensional ($d = 2$) ensemble-averaged mean-squared displacement (MSD) of the particles undergoing Brownian motion over time, τ [24,25]. Unlike active (nonlinear) microrheology methods that measure the response of a probe particle to an external force (e.g., driven magnetically), passive measurements use only the thermal energy of embedded colloids to measure rheological properties in the linear viscoelastic (LVE) region. Viscous fluids show irreversible deformations to stress, whereas elastic materials return to their original shape after the removal of stress. Equation (1) shows that the MSD is directly proportional to the macroscopic creep compliance of the material, i.e., its tendency to deform permanently over time. In the limit for a spherical Brownian particle diffusing within a Newtonian solution of viscosity η_0, $J = \tau/\eta_0$ and the GSER simplifies to the Stokes–Einstein–Sutherland equation

$$\eta_0 = \frac{dk_B T}{3\pi a\langle \Delta r^2(\tau)\rangle}\tau. \tag{2}$$

Under such conditions, probes exhibit diffusive trajectories characterized by $\langle \Delta r^2 \rangle \propto \tau$ (purely viscous response). In viscoelastic systems, the MSD exhibits an emerging dependence on lag time; typically a power-law scaling, $\langle \Delta r^2 \rangle \propto \tau^\alpha$, where α is the diffusive (or power-law) exponent. Subdiffusive behavior ($0 < \alpha < 1$) initially occurs at early lag times and the MSD exhibits a crossover to diffusive behavior ($\alpha = 1$) at longer lag times. If that is the case, viscosity can be evaluated at the purely viscous long-time slope of the MSD using Eq. (2). Subdiffusive behavior at short lag times reflects an elastic response arising from particle entanglement in the molecular network, due to the relaxation of the Rouse-like fluctuations of its macromolecules. Thus, an increase in the longest relaxation time λ is evident by the increase in time required for the MSD scaling to recover to unity, ultimately exhibiting a power-law dependence over all times and subsequent dynamics from increased entanglements in more crowded solutions.

As long as the length scale of the probes is much larger than the characteristic mesh size of the network in the complex fluid, bulk rheology can be inferred from the passive bead trajectories using the real and imaginary components of the frequency-dependent complex shear modulus $G^* = G' + iG''$ and Euler's formula with

$$G^*(\omega) \sim \frac{dk_B T \exp[i\pi\alpha(1/\omega)/2]}{3\pi a\langle \Delta r^2(1/\omega)\rangle \Gamma[1+\alpha(1/\omega)]}, \tag{3}$$

where Γ designates the gamma function, $\omega = 1/\tau$ is angular frequency, and α is the aforementioned logarithmic slope assumed for the MSD [26]. Herein, we employ the algebraic approximation to the GSER proposed by Dasgupta *et al.* [27], which—despite more robust than Eq. (3)—is also based on power-law approximations of the data.

All the fluids were seeded with approximately 0.05% (w/w) of 3 μm (nominal) radius poly(methyl methacrylate) (PMMA) probe particles (Spheromers CA6, Microbeads AS). The mean particle diameter in our lot is 6.1 μm and their density (ρ_p) is 1.2 g ml^{-1}, as given by the manufacturer. Tracers naturally probe viscoelasticity on length scales comparable to their size, i.e., depending on mesh size, smaller particles might only measure Brownian motion where larger ones measure the viscoelasticity that represents the bulk rheology [28–30]. The choice of such large probes was not only to make sure that the medium was treated as a continuum and ensure the GSER's validity[4] but also to promote slow diffusion and prevent dynamic error in the MSD (more on that in Sec. S1 of [31]). The probing was carried out shortly after the introduction of the beads in an attempt to avoid prolonged sedimentation (see Sec. S2 of [31] for details on accounting for probe-wall hydrodynamic interactions). A poly(ethylene oxide) (PEO) aqueous solution is used to validate the experimental microrheology setup (Sec. S3 of the supporting information in [31]).

A fluid volume of roughly 260 μl was then loaded into the sample chamber (137-1-40, Hellma Analytics) and its in/outlets were sealed. Both fluid and ambient temperatures were monitored by taking readings immediately before and after each measurement using a standard thermocouple. The

[4]Again, in order to measure continuum viscoelasticity and extract bulk properties, the colloidal particles must be larger than all the structural length scales of the material.

mean fluid temperature inside the chamber at ambient conditions (T_{ref}) was $20.9 \pm 1.9\,^{\circ}\mathrm{C}$ (averaged across all experiments), with the room temperature being $20.0 \pm 1.3\,^{\circ}\mathrm{C}$ (2-sigma error). The optical setup consisted of an inverted microscope (DM IL LED, Leica) equipped with a $63\times$ magnification and NA $= 0.7$ numerical aperture objective (HCX PL FLUOTAR L, Leica). Once the loaded sample was assumed stationary, particle displacements were tracked using a high-speed CMOS camera (FASTCAM UX100, Photron) in a field of view and depth of focus of about $123 \times 123 \times 1\text{–}2\,\mu\mathrm{m}$ (at $0.16\,\mu\mathrm{m\,px^{-1}}$ magnification) at a rate of $f = 125$ fps and $\phi = 8$ ms exposure time (i.e., shutter speed) for 3750 frames ($\equiv$30 s). Measurements of BP at body temperature (T_{body}) were performed on top of a heated glass plate (TPi-SQMX, TOKAI HIT) positioned on the microscope's stage and connected to a temperature control unit (MATS, Leica) that kept the biofluid at $38.0 \pm 2.0\,^{\circ}\mathrm{C}$ (average $\pm 2\sigma$ across all experiments; negligible temperature gradients, $<1\,^{\circ}\mathrm{C}$, measured during probing).

The trajectories of the colloidal particles were tracked using the routines developed by Crocker and Grier [32] (and implemented alongside Weeks and a few others). The random walks measured were dedrifted to prevent convective drift from affecting the results and particle–particle interaction artifacts were avoided by only tracking probes reasonably far away from each other. Static and dynamic particle tracking errors were accounted for in the data, as detailed in Sec. S1 [33]. Multiple local microenvironments were probed and individually checked for heterogeneity within each sample loaded so that the (here similar) Brownian dynamics characterizing the different probing sites could be combined into a single second-order ensemble average (i.e., MSD) in order to increase statistical accuracy and better investigate heterogeneity. Figure 3 illustrates this technique as well as the MPT microrheology framework employed, from the loading of samples into the chamber to the determination of rheological properties from the two-dimensional random walks tracked.

The viscosity η_0 of the BP and protein solutions was extracted from the purely viscous long-time slope of the MSDs using Eq. (S7). The operating regime of our passive microrheology system limits the MSD lag times between $\tau_{\mathrm{min}} = 1/f$ and the somewhat arbitrary τ_{max} [for which we found some meaning in Sec. III A; see Figs. 4(a) and 4(c)] [34]. Viscosity flow curves were obtained for BP using a rotational rheometer (Kinexus pro, Malvern) fitted with PD and concentric cylinder (CC) fixtures. A Peltier-controlled

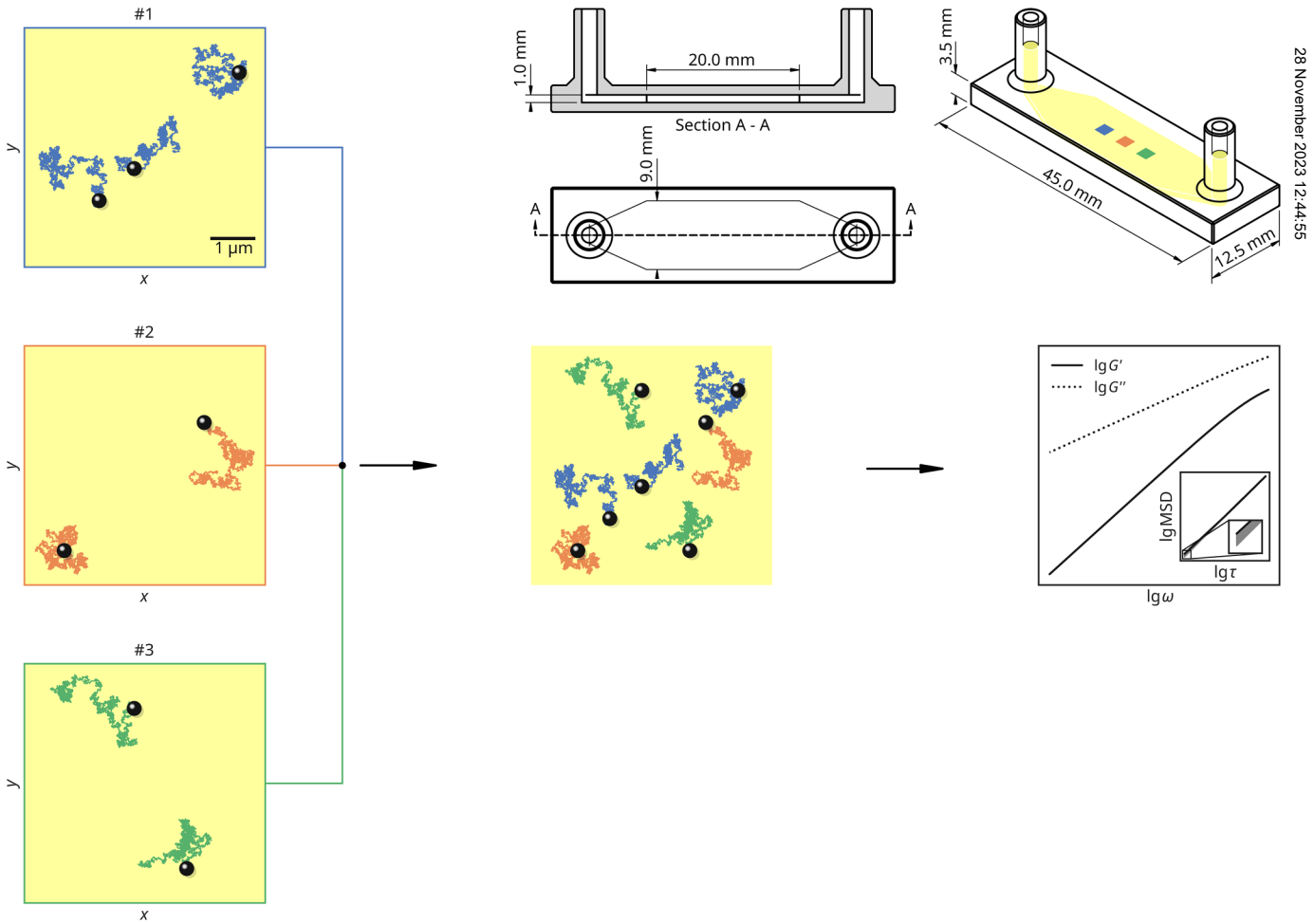

FIG. 3. Schematic illustrating the passive microrheology framework (probes are not to scale). Multiple Brownian particle trajectories measured within the sample chamber are ensemble-averaged together to increase statistical accuracy. Likewise, the combined MSD introduced in Sec. III A was calculated from particle displacements tracked in the plasma samples #1, #2, and #3.

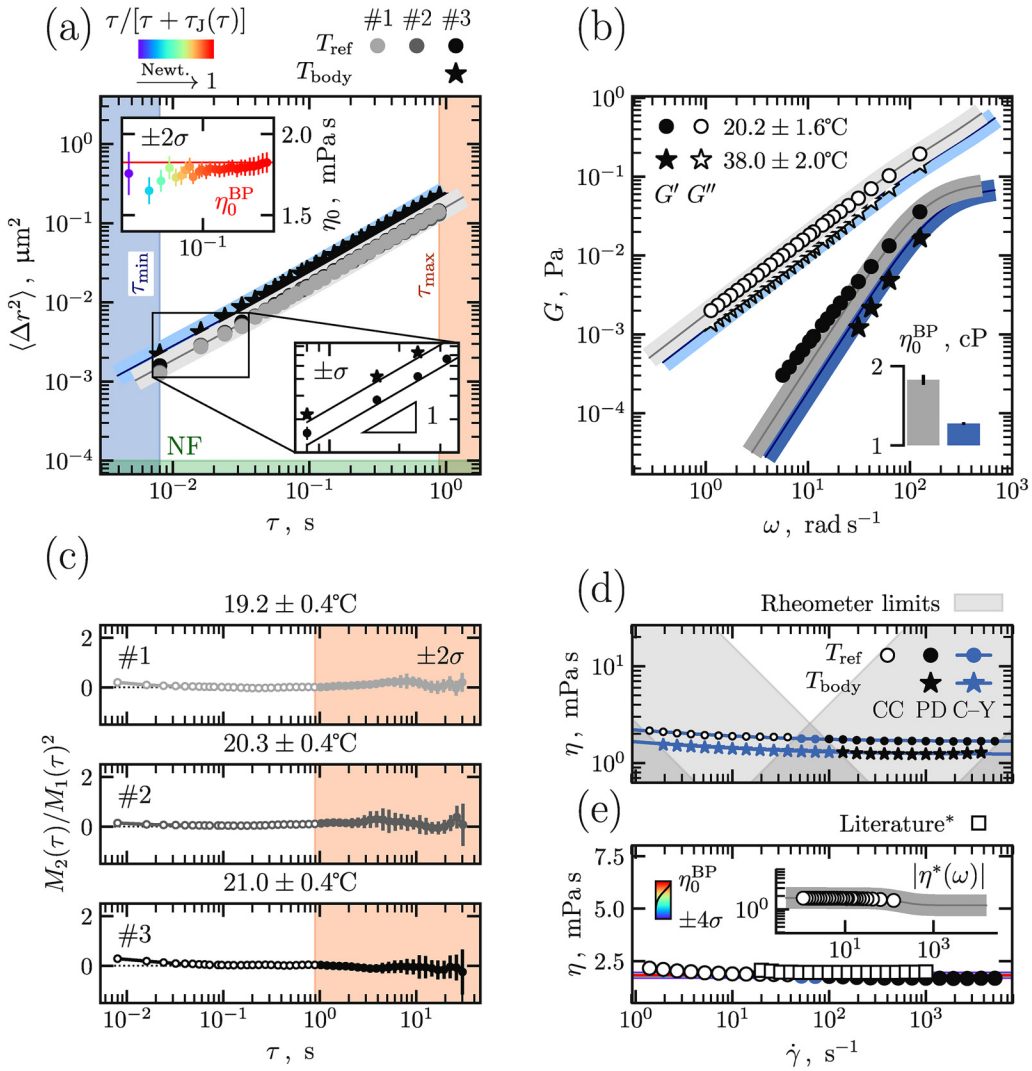

FIG. 4. Rheological characterization of human blood plasma at 20 and 37 °C. (a) MSD as a function of lag time τ. (Upper inset) Viscosity obtained using Eq. (S7) is plotted as a function of τ for the multisample MSD (20 °C). η_0^{BP} is extracted from the long-time limit of the MSD, where $\tau/(\tau+\tau_J)$ approaches unity. (Lower inset) Subdiffusive deviation from the Newtonian profile at the shortest lag times. (b) Real and imaginary parts of the inferred complex shear moduli G^*. (Inset) η_0^{BP} at 20 and 37 °C (two-sigma error bars). (c) Ensemble scaled variance of the MSDs measured in each sample. [(d) and (e)] Steady shear rheology of BP compared to (*) literature [5]. The C–Y fits (with parameters $\eta_0^{C-Y} = 4.64$ mPa s, $\dot{\gamma}^{C-Y} = 1.39\ s^{-1}$, $n = 0.35$, and $a = 0.24$ at 20 °C) are shown in blue in the online figure. [Inset of (e)] Complex viscosity's magnitude as a function of angular frequency. The gray lines (online figure) in (a), (b), and (e) correspond to the complex moduli of a Jeffreys fluid ($\tau_c = 6.88$ ms, $\eta_0 = 1.80$ mPa s, and $\upsilon = 4.68$ ms at 20 °C).

hood kept the fluid temperature constant (20 and 37 °C) and prevented its evaporation. Whenever conventional bulk rheology measurements are presented, the relevant mechanical and sample-related experimental limits of shear rheometry are plotted: low-torque limit and secondary flow effects for steady shear data, and instrument inertia effects for SAOS data [Figs. S2 and 4(d), shaded regions] [35].

III. RESULTS AND DISCUSSION

We now present a detailed description of the main findings drawn from the data gathered, purposely introduced and commented on in two separate instances matching both the experimental and conceptual tempos of the investigation: in Sec. III A, we extend the current knowledge about the rheology of BP with more complete and novel datasets of shear flow material functions, adding to the many proofs of its (subtle) viscoelastic nature; in Sec. III B, we investigate if individual and mixed plasma proteins at normal concentration in PBS convey measurable elasticity to the bulk.

A. Rheological characterization of human blood plasma

As previously mentioned, human BP collected from three different donors was used in the experiments. The MSDs measured in each sample are shown in Fig. 4(a) and are qualitatively described by a three-parameter Jeffreys fluid model (parameters provided in the caption of Fig. 4), rather than by the typical power-law scaling.[5] The MSD of a bead in a

[5]This model is a generalization of the classic Maxwell fluid for the case of additional viscous contributions during high-frequency ($\omega\tau_c > 1$) probing, using the parameter υ. Notationwise, it is henceforth presented in one of its two possible spring-and-two-dashpots configurations.

Jeffreys fluid yields from the Langevin equation [36] (that shortly followed Einstein's theory of Brownian motion) and has been used to describe the Brownian dynamics of microspheres in soft materials before [37]. In fact, both Maxwell and Jeffreys models have proven very useful theoretical tools for gaining insight into the qualitative effects of viscoelasticity on Brownian motion [15,37,38]. For ease of understanding, we present first the formula for the creep compliance J in a Jeffreys fluid and only then the MSD. Hence, the former can be written in a Maxwellian form as

$$J(\tau) = \frac{1}{\eta_0}[\tau + \tau_J(\tau)], \tag{4}$$

with the physically meaningless[6] equivalent of the characteristic Maxwell relaxation time τ_c for the Jeffreys fluid being

$$\tau_J(\tau) = (\tau_c - \upsilon)\left[1 - \exp\left(-\frac{\tau}{\tau_c}\right)\right], \tag{5}$$

where υ is the retardation time characteristic of its additional dissipation mechanism (or dashpot), i.e., the background solvent's viscosity [38,39]; finally, from Eqs. (4) and (5) comes (for $\tau \neq 0$)

$$\begin{aligned}\left\langle \Delta r^2(\tau)\right\rangle &= \frac{dk_BT}{3\pi a}J(\tau) = \underbrace{\frac{dk_BT}{3\pi a\eta_0}}_{\Delta_0^2/\tau_J(\tau)}[\tau + \tau_J(\tau)] \\ &= \underbrace{\frac{dk_BT}{3\pi aE_0^J(\tau)}}_{\Delta_0^2}\left[1 + \frac{\tau}{\tau_J(\tau)}\right].\end{aligned} \tag{6}$$

Looking at Eq. (6), it becomes clear that $\eta_0 = E_0^J\tau_J$ and that the MSD has a slope of $2dD = \Delta_0^2/\tau_J$ (D is the diffusion coefficient) and an offset (i.e., the y-intercept at $\tau = 0$) of Δ_0^2. Here, E_0^J can be regarded as the physics-wise meaningless[6] equivalent of Maxwell's short-term shear modulus $E_0^M = \eta_0/\tau_c$.

The increasing subdiffusive deviation from the Newtonian linear slope of $4D$ at the shortest lag times (heading toward the offset Δ_0^2 as $\tau \to 0$) is indicative of an elastic response to the Brownian motion-induced shear stress [12,28], being tied to the relaxation of proteins in solution [13,15,16]. The probe particles end up interacting with the protein molecules at these timescales via the viscoelastic dynamics of the molecular network that they compose, which in turn influences particle motion. This deviation can be quantified by taking the ratio between the MSD of a diffusing bead in a viscous fluid and in a Jeffreys fluid [Eq. (6)], which gives $\tau/(\tau + \tau_J)$. At body temperature, the curvature in the MSD is less apparent and for even shorter lag times (faster relaxation) [5]. The working range of our microrheology setup boxes the MSDs measured within the bounds NF, τ_{min} and τ_{max} (introduced in Secs. II B and S1 of [31]), which are shown in Fig. 4(a) for clarity [the upper limit τ_{max} on the MSD lag times shall be better understood upon discussion of Fig. 4(c)].

Since the particles tracked in the three BP samples displayed identical dynamical signatures (each sample was checked for heterogeneity) and the fluid temperature measured across these experiments never exceeded a 2-sigma error of $\pm 1.6\,^{\circ}C$ (of the mean $20.2\,^{\circ}C$), a multisample MSD was computed with all the trajectories. From the long-time slope of this MSD [where the behavior is purely viscous and $\tau/(\tau + \tau_J) \sim 1$], the zero-shear viscosity of human plasma (η_0^{BP}) at reference temperature was estimated at 1.82 ± 0.12 mPa s, as depicted in the upper inset of Fig. 4(a) (here, the four-sigma error was propagated from the uncertainty affecting the ensemble-averaged MSD: its variance σ^2; reflecting the influence of the individual MSDs calculated from time-averages over each trajectory considered). Note that the error in the viscosity is rather small—even more so considering that it is a four-sigma error, encapsulating essentially the entire Gaussian distribution that one may construct from it [see Fig. 4(e)]—which is a measure of the degree of the statistical accuracy characterizing the MSDs calculated.

Having obtained the trajectories of colloidal spheres embedded in the different BP samples and ensemble-averaged them into a single MSD, we measured the frequency-dependent complex shear modulus G^* of the biofluid. The data are shown in Fig. 4(b), showcasing a dominant viscous response ($G'' > G'$) seemingly all throughout the frequency domain. The behavior of the moduli is, again, reminiscent of a Jeffreys model thanks to the background viscosity η_∞ that differentiates it from the single-relaxation-time Maxwell fluid, preventing G'' from plunging at frequencies greater than $1/\tau_c$ unlike the latter (which does not account for the dissipation in the solvent) [38]. Near this angular frequency ($\omega\tau_c \sim 1$)—according to the Jeffreys fluid model—the magnitude of the dynamic complex viscosity $|\eta^*|$ shear-thins (for $\tau_c > \upsilon$) from η_0 to η_∞. For this type of fluid, the frequency-dependent real and imaginary parts of G^* read

$$G^*(\omega) \to \begin{cases} G'(\omega) = \eta_0\omega\left[\frac{(\tau_c - \upsilon)\omega}{1+\tau_c^2\omega^2}\right] \\ G''(\omega) = \eta_0\omega\left(\frac{1+\tau_c\upsilon\omega^2}{1+\tau_c^2\omega^2}\right)\end{cases}, \tag{7}$$

respectively. The zero-shear viscosity is η_0 and the plateau one is $\eta_\infty = \eta_0\upsilon/\tau_c$. The plateau modulus of the Jeffreys fluid is found by doubling the storage modulus evaluated at angular frequency $1/\tau_c$ (the crossover frequency ω_c in a Maxwell fluid),

$$G_p = 2G'(1/\tau_c) = \frac{\eta_0(\tau_c - \upsilon)}{\tau_c^2} = \frac{E_0}{E_0^M}, \tag{8}$$

where E_0 is Jeffreys' actual short-term shear modulus, which yields from its time-dependent relaxation modulus,

$$E(\tau) = \frac{\eta_0}{\tau_c}\left[\upsilon\tau + \frac{\eta_0}{\tau_c}\left(1 - \frac{\upsilon}{\tau_c}\right)\exp\left(-\frac{\tau}{\tau_c}\right)\right] \tag{9}$$

at $\tau = 0$ [39]. Doing likewise for the Maxwell model ($\upsilon = 0$)

[6]Considered solely for explanatory purposes as a function of time τ.

yields a simpler expression for its plateau modulus,

$$G_{\mathrm{p}}^{\mathrm{M}} = 2G'_{\upsilon=0}(\omega_{\mathrm{c}}) = 2G''_{\upsilon=0}(\omega_{\mathrm{c}}) = \frac{\eta_0}{\tau_{\mathrm{c}}}$$
$$\therefore \quad G'_{\upsilon=0}(\omega_{\mathrm{c}}) = G''_{\upsilon=0}(\omega_{\mathrm{c}}) = G_{\mathrm{c}}^{\mathrm{M}}, \tag{10}$$

where $G_{\mathrm{c}}^{\mathrm{M}} = G_{\mathrm{p}}^{\mathrm{M}}/2$ is the crossover modulus and $G_{\mathrm{p}}^{\mathrm{M}} = E_0^{\mathrm{M}}$.

The medium's elastic response to the Brownian probes is characterized by the storage modulus G', which is related to the curvature of the MSD's leftmost part (where protein relaxation is felt). To the best of the authors' knowledge, this modulus constitutes the first experimental evidence of bulk elasticity under shear in normal BP. Together with the loss modulus G'', the moduli quantify the linear viscoelasticity of the complex biofluid. Varchanis *et al.* [9] estimated the crossover from elastic to viscous behavior—here, also the intermediate regime bridging the short- to the long-time diffusion—at a time constant of order 0.09 ms (the point at which a pronounced deviation from the terminal scaling $G' \propto \omega^2$ is observed), but predicted lower values for the elastic modulus of BP by comparison with the present results.

Figure 4(c) quantifies the spatial heterogeneity of each BP sample according to the method developed by Savin and Doyle [40]. The heterogeneity ratio (termed by Rich *et al.* [41])

$$\mathrm{HR} = \frac{M_2(\tau)}{M_1(\tau)^2} \tag{11}$$

is a dimensionless number defined as the ratio of the ensemble variance to the square of the ensemble mean of the individual MSDs, where M_1 and M_2 are estimators for $\langle \Delta x^2 \rangle$ and $\langle \Delta x^4 \rangle/3 - \langle \Delta x^2 \rangle^2$, respectively, in one dimension (with $\langle \Delta x^4 \rangle$ being a fourth-order ensemble average, or moment). M_2 is, therefore, a measure of how spatially disperse the particle dynamics are in a material since the probing is performed locally in multiple positions within the sample. Figure 4(c) also highlights the cut-off lag time above which discrepancies are observed in the ensemble-averaged MSDs, here used as the upper working limit $\tau_{\max}$. To the left of $\tau_{\max}$ we observe evidence of BP being homogeneous (HR $\sim$ 0). One can then expect that all the particles displayed similar dynamical signatures (i.e., MSDs) no matter their probing site, suggesting that the spatial distribution of material properties in human BP is uniform and the biofluid is isotropic. This explains the use of a passive probing technique based on the motion of single particles, rather than pairs (the latter is particularly useful for probing heterogeneous media) [42]. Alternative methods of quantifying heterogeneity do exist, the most common being the van Hove analysis of the probability density functions (PDFs) of particle displacements at selected lag times—which should be Gaussian if the medium is homogeneous [41,43], corresponding to classical random walk statistics (measured in Cartesian coordinates) [44].

The flow curves shown in Fig. 4(d) add to the steady shear rheology of BP presented in Brust *et al.* [5] [shown in Fig. 4(e)] by covering a wider shear rate spectrum at both reference and body temperatures ($T_{\mathrm{ref}} = 20\,^{\circ}\mathrm{C}$ and $T_{\mathrm{body}} = 37\,^{\circ}\mathrm{C}$, respectively), while also revealing a mild shear-thinning character. At reference temperature, the shear rate-dependent viscosity of the biofluid was measured using two different geometries (see Sec. II B for details) so as to maximize the range of the shear rate ramp swept, albeit a small gap outside the experimental limits could not be accessed. To fill this gap, the Carreau–Yasuda (C–Y) generalized Newtonian fluid (GNF) was used to model the slight shear-thinning of the flow curve,

$$\eta = \eta_\infty + \left(\eta_0^{\mathrm{C-Y}} - \eta_\infty\right)\left[1 + \left(\frac{\dot\gamma}{\dot\gamma^{\mathrm{C-Y}}}\right)^a\right]^{\frac{n-1}{a}}, \tag{12}$$

where $\eta_\infty = 1.67$ mPa s (Table II) and $\eta_0^{\mathrm{C-Y}}$, $\dot\gamma^{\mathrm{C-Y}}$, a and n are the best-fit zero-shear viscosity, characteristic shear rate for the onset of shear-thinning, zero-shear (or Newtonian) plateau to power-law region transition parameter ($0 < a < 2$; doing $a = 2$ yields the Carreau model) and power-law index ($0 < n < 1$; doing $n = 1$ yields a Newtonian fluid with viscosity $\eta_0^{\mathrm{C-Y}}$), respectively [45]. The model—which describes the flow curve at 20 °C well—was then used to infer the viscosity at 37 °C for shear rates to the left of those swept using the PD measuring geometry. To do so, the time-temperature superposition (TTS) principle with a shift factor of

$$a_{\mathrm{T}} \sim \frac{\eta_\infty^{T_{\mathrm{body}}}}{\eta_\infty^{T_{\mathrm{ref}}}} \quad \because \quad |\delta\eta| \gg |\delta(T\rho)| \tag{13}$$

(here, δY means a temperature-driven change in the value of Y) was employed, assuming that BP is a "thermorheologically simple" fluid [46]. The C–Y model of Eq. (12) defined at 20 °C (parameters provided in the caption of Fig. 4) can, thus, be shifted along both axes to 37 °C by plotting the reduced viscosity ηa_{T} against the reduced shear rate $\dot\gamma/a_{\mathrm{T}}$. As expected, the shifted curve matches the steady shear data measured with the PD geometry and does a good job at predicting the seemingly shear rate-dependent viscosity at lower shear rates, based on the complete flow curve that Eq. (12) was modeled after. The same (timescale) factor a_{T} and an additional one, b_{T} (determined empirically), were used to shift the Jeffreys model that describes the MSD and frequency-dependent moduli of BP at T_{ref} along their corresponding x and y axes, respectively, to T_{body} [Figs. 4(a) and 4(b), gray and blue lines in online figure]. This way, the shift factors a_{T} and b_{T} collapse the MSD, moduli, and shear viscosity data measured at reference and body temperatures onto single master curves (not shown) using the appropriate scaling laws [47].

Figure 4(e) shows the steady shear rheology of BP (sample #3) measured at reference temperature, compared to the dataset presented in Brust *et al.* [5]. Moreover, the Gaussian (or normal) PDF of the zero-shear viscosity η_0^{BP} extracted from the MSD is displayed (up to $\pm 4\sigma$), as well as the frequency-dependent complex viscosity's magnitude $|\eta^*| = |G^*|/\omega$ [determined from the moduli in Fig. 4(b)] and its corresponding Jeffreys fit. All the viscosity functions

shown are in good agreement with each other—including $|\eta^*|$ as a function of ω, which can be compared to the rest using the rule of Cox–Merz [48] (the inset shares the units of the parent axes)—supporting the correctness of the results presented.

Although not the first, Castellanos *et al.* [49] and Gudapati *et al.* [50] reported that under steady shear flow, globular (e.g., albumin and immunoglobulins) and fibrous (e.g., fibrinogen) proteins, respectively, display an apparent low shear viscosity increase as a result of protein adsorption to the solution/air interface. This produces a shear-thinning flow curve that is an artifact of the interfacial phenomena taking place, which can be countered, for instance, with the addition of surfactants. The subtly decreasing viscosity with shear rate that we measured for BP [Figs. 4(d) and 4(e)] could be ascribed to the surface-induced distorted bulk response just-mentioned, despite Ariola *et al.* [51] having reported no such surface elasticity in serum. Nevertheless, to mitigate such artifacts, we used a concentric cylinder (or single gap Couette) measuring geometry to sweep the low-end (roughly 1–100 s^{-1}) of the shear rate range investigated, which is the best for this purpose according to Zhang *et al.* [52]. Protein aggregation in the bulk also promotes low shear viscosity increase, and we find this more likely to be the cause here [49,53]. In fact, both agitation and shear are known to promote protein aggregation [54].

B. Plasma proteins microrheology

We performed passive microrheology on plasma proteins —namely, albumin (BSA), fibrinogen (Fg), and

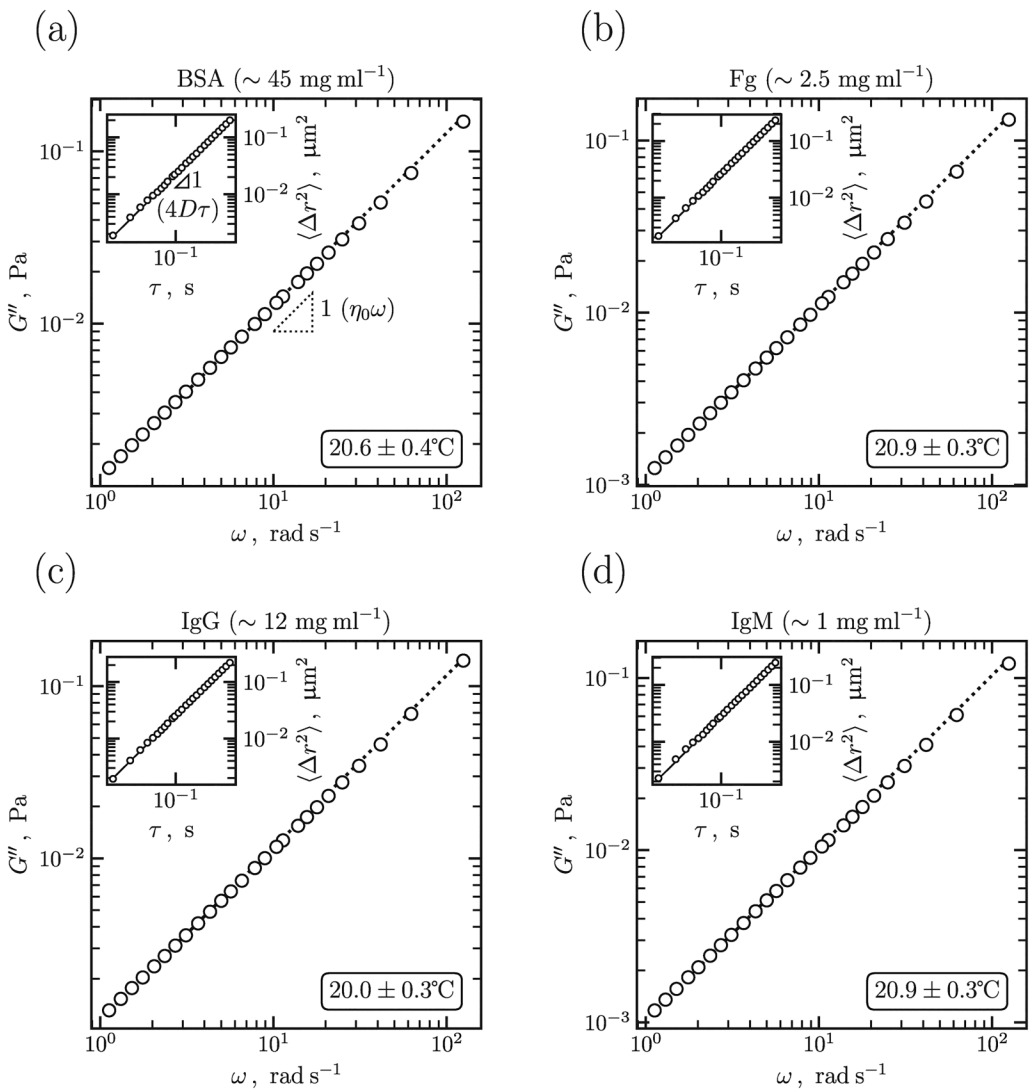

FIG. 5. Passive microrheology of selected plasma proteins in PBS at reference temperature. [(a)–(d)] Loss modulus is shown as a function of angular frequency ω for single proteins in solution. Dotted lines indicate Newtonian fluid behavior. [(e)–(g)] Shear moduli as a function of ω for solutions with multiple dissolved proteins. [Insets of (a)–(g)] MSD as a function of lag time. Solid lines indicate simple diffusion. (h) Scaled shear moduli are plotted as a function of scaled angular frequency for BP and solutions γ-g, M1, and M2. (Inset) Normalized MSD as a function of normalized lag time. The data collapse onto a single master curve, given by Eq. (6). (i) Viscosity η_0 of the protein solutions. (j) Cole–Cole plot for viscosity (for the Jeffreys model this is a semicircle). All inferred shear moduli were approximated using Eq. (3). Gray and colored lines (online figure) in (e)–(h) and (j), respectively, represent the rheological response of a Jeffreys fluid.

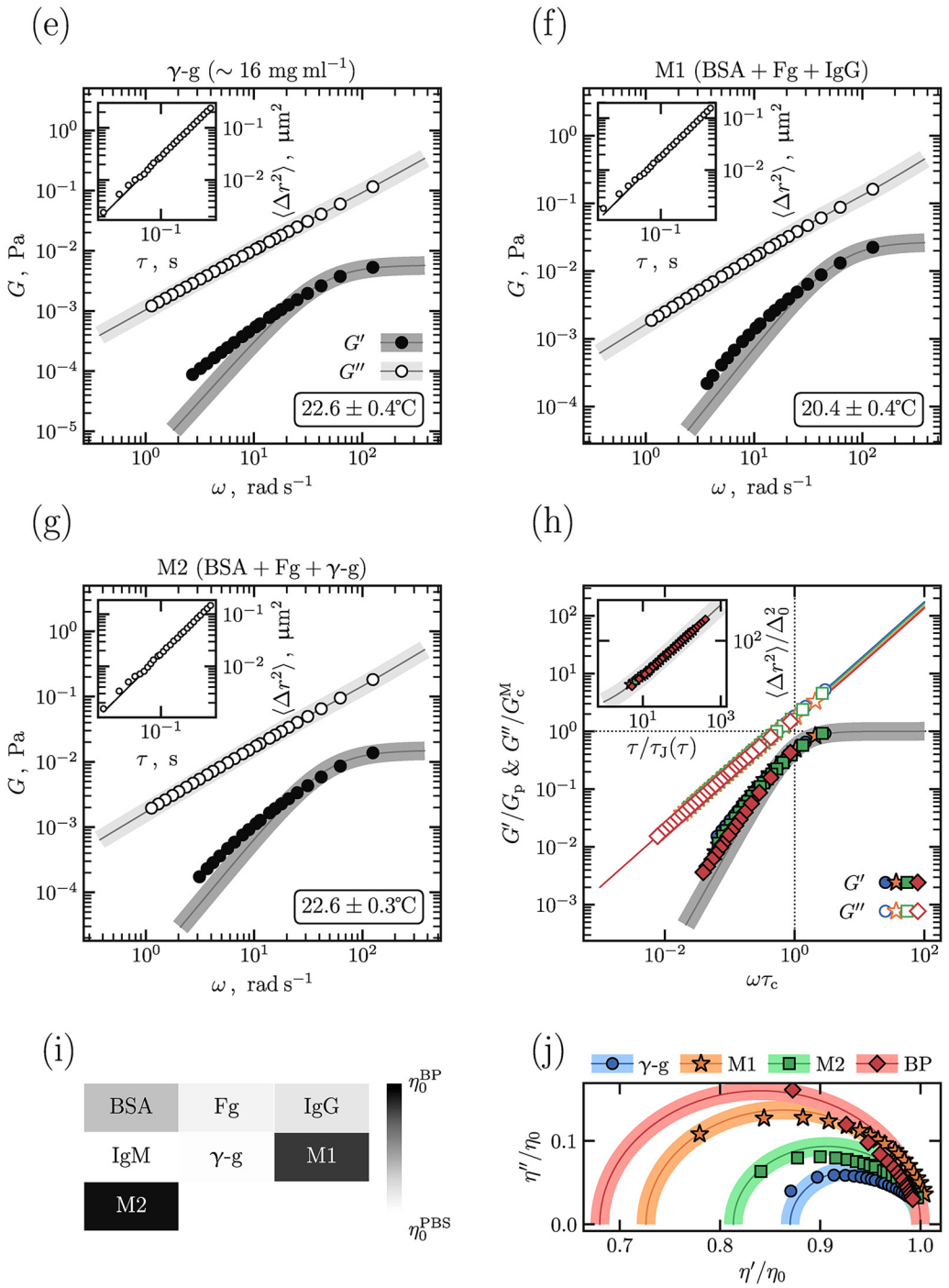

FIG. 5. (*Continued.*)

immunoglobulins G (IgG) and M (IgM),[7] at physiological concentrations—individually and mixed together in PBS (Fig. 5). All the single protein solutions investigated exhibited Newtonian behavior: a linearly growing MSD $\propto \tau$ and resulting viscous shear modulus $G'' \propto \omega$ [Figs. 5(a)–5(d)]. Conversely, the protein mixtures probed [Figs. 5(e)–5(g)] showcased MSDs subtly subdiffusing off the simple diffusion profile at the shortest lag times, resembling those obtained for the BP samples [Fig. 4(a)]. Consequently, from the MSDs measured, loss and storage moduli were computed.

The MSD and storage and loss moduli that reveal viscoelasticity (solutions γ-g, M1 and M2) are, too, qualitatively described by the Jeffreys fluid model (gray lines in online figure). Least-squares fits (with a Powell minimization algorithm) were used when fitting Eqs. (6) and (7) to the MSD and viscoelastic shear moduli experimental data, respectively, likewise the Jeffreys fit to the BP datasets [Figs. 4(a), 4(b), and 4(e) (inset), gray lines in online figure]. In Fig. 5(h), we

[7]A mixture of gamma-globulins (γ-g) containing IgG, IgM, and IgA (according to the supplier) was also used, as detailed in Sec. II A.

collapse the MSD and inferred moduli measured in BP and solutions γ-g, M1 and M2 onto master curves, accordingly: the individual MSDs are scaled by their respective Δ_0^2 and τ_J—see Eq. (6)—so that each collapses onto the normalized diffusive behavior in a Jeffreys fluid, $\langle \Delta r^2 \rangle / \Delta_0^2 = 1 + \tau/\tau_J \Leftrightarrow y = 1 + x$; to collapse the moduli G datasets approximated using the GSER onto normalized Jeffreys storage and loss moduli master curves, the frequency axis was scaled by τ_c, the elastic modulus axis by G_p, and the viscous modulus axis by G_c^M. This way, we end up with a MSD master curve with an offset and slope of unity, and G master curves with a plateau modulus and characteristic time of unity as well. By superposing the experimental data in this manner, the Jeffreys-like rheology of the fluids in question stands out. For frequencies roughly above $1/\tau_c$, the dimensionless loss modulus branches into four curves (each corresponding to one of the fluids). This branching can be quantified by taking the ratio between the retardation and relaxation times $[0 < (\upsilon/\tau_c = \eta_\infty/\eta_0) < 1]$: here, all the way from 1 for a Newtonian fluid—where $\upsilon = \tau_c$ and the complex shear modulus is strictly imaginary according to Eq. (7) (υ and τ_c cancel one another out), resulting in a linear parent branch (not shown)—to approximately 0.68 for BP (the outer branch).[8]

In Fig. 5(i), we rank the protein solutions according to their long-time zero-shear viscosity η_0 extracted from the MSD, from a minimum of η_0^{PBS} (solvent) to a maximum of η_0^{BP}. We find that the viscosities rank as expected, proportional mainly to protein concentration but also molecular weight (except for solution γ-g, likely a consequence of the temperature). Higher concentrations promote particle entanglement in the molecular network, thereby restricting particle motion. We highlight the yellowish color of solution M2, the one that resembles BP the most in terms of protein composition. A Cole–Cole plot was graphed to compare the protein solutions that revealed viscoelasticity and BP, in terms of the magnitude of their viscous (G'') and elastic (G') components [Fig. 5(j)]. For a Jeffreys fluid, we found that the Cole–Cole plot for viscosity is semicircular. We also found that the same rainbowlike pattern observed in the branching of the normalized loss modulus [Fig. 5(h)] is recovered in the semicircles' radii. Interestingly, the relation between the Newtonian plateau viscosities $\eta_0^{BP} > \eta_0^{M2} > \eta_0^{M1} > \eta_0^{\gamma\text{-g}}$ drawn from the purely viscous long-time slope of the MSDs, is not reflected in the semicircles' radii. The reason is that the construction of a Cole–Cole plot from, in this case, the complex viscosity's $\eta' = G''/\omega$ and $\eta'' = G'/\omega$ parts (scaled by η_0, here estimated at long times using η') encompasses the entire diffusive behavior captured by the MSD, including the subdiffusive dynamics at short times $\tau \lesssim \tau_c$ (or high frequencies $\omega \gtrsim 1/\tau_c$). Therefore, the different radii give information on the viscoelasticity of the fluids (which can possibly be estimated by the short-term elastic modulus inferred from the passive Jeffreys rheology: $E_0^{BP} > E_0^{M1} > E_0^{M2} > E_0^{\gamma\text{-g}}$). The pattern observed in the branching of the dimensionless loss modulus for the Jeffreys fluids [Fig. 5(h)] was found to repeat itself at least in the semicircles' radii of the Cole–Cole plots [Fig. 5(j)], in the ratio between the retardation and relaxation times (υ/τ_c), in the short-term elastic modulus (E_0), and in the degree of anomalous diffusion exhibited by the MSDs for $\tau \lesssim \tau_c$, and agrees well with the slopes of the MSDs at shorter lag times ($\alpha_{BP} < \alpha_{M1} < \alpha_{M2} < \alpha_{\gamma\text{-g}} < 1$) and inferred moduli determined by the passive microrheology.

From the zero-shear viscosities and Cole–Cole plots presented in Figs. 5(i) and 5(j), respectively, one concludes that despite the higher protein concentration of solution M2 compared to M1 ($\eta_0^{M2} > \eta_0^{M1}$), the former exhibits less viscoelasticity ($E_0^{M2} < E_0^{M1}$). Perhaps a temperature effect could explain this; however, do note that the viscoelastic shear moduli inferred are estimates based on a power-law approximation to the MSD [Eq. (3)], which is not the best for the frequency response expected for Jeffreys [Eqs. (6) and (7)] or Maxwell [Eqs. (6) with $\tau_J = \tau_c$ and (7) with $\upsilon = 0$] models [15].

Ultimately, we have considered the viscoelastic dynamics of the protein systems investigated analogous to those of polymer solutions, i.e., protein molecules adopting random coil chain conformations and contributing to the complex rheology of the bulk in a similar fashion. Based on our findings, we see no likelihood of single plasma protein solutions at physiological concentrations displaying measurable elastic behavior in the small deformations regime of LVE. The same concentration of BSA in water measured by Brust *et al.* [5] under extensional flow (despite more accurate techniques for measuring protein extensional rheology having appeared since [55]) exhibited a Newtonian response in our experiments as well. Nevertheless, the unraveling or self-associating properties of individual plasma proteins may still very well have a profound influence on the elasticity of the whole [9,53,56].

Unlike in BP, the role of protein content on bulk rheology has been widely investigated in synovial fluid [13,52,57,58]. The formulation of analog solutions (model synovial fluids) composed of hyaluronic acid—the polysaccharide mainly responsible for the viscoelasticity of the joint lubricant—and plasma proteins—such as albumin, immunoglobulins, and fibrinogen—is also common practice. However, besides a number of the protein-driven viscoelastic phenomena reported having been later attributed to interfacial rheology (of the kind already mentioned) [49–51], most of the data concerning the little to no effect of plasma proteins on synovial fluid's bulk properties were obtained by macroscopic mechanical rheology or microfluidic rheometry measurements [52,57], hence lacking the fine-grained probing capabilities of Brownian tracers. For instance, Jay *et al.* [13] used MPT microrheology to demonstrate that lubricin-deficient synovial fluid lacked the short-term elasticity that the MSD of colloidal particles diffusing through normal synovial fluid revealed. Just like lubricin (PRG4) affects the rheology of synovial fluid—despite its scarce abundance (at a concentration of about an order of magnitude lower than IgM's in BP) and IgG-like molecular weight—selected plasma proteins could, too, be promoting the non-Newtonian behavior of BP.

The fact that the 45 mg ml^{-1} BSA solution exhibited purely viscous behavior over all lag times and the γ-g

[8]A ratio of zero would imply $\upsilon = 0$, i.e., the single-relaxation-time Maxwell fluid, which has no solvent plateau viscosity η_∞.

solution at 16 mg ml^{-1} (and lower viscosity) did not, indicates that protein concentration alone does not account for the elastic response under physiological conditions. Thus, we are led to consider other possible origins of the weakly elastic behavior observed. In addition to the protein concentration, molecular weight, and/or extensibility effects, we can also give another interpretation of the present results: the formation of protein complexes promoted by protein–protein interactions (PPIs). Similar works have attributed subdiffusive behavior in the MSD to protein binding before, which correlates with bulk elasticity via the enhanced flexibility of the network-forming bound molecules [13,16]. Although it is not far-fetched to suggest that protein complexes may explain the occurrence of anomalous diffusion at short times, it cannot be assumed *a priori* and only seldom has it been experimentally verified among plasma proteins [53,56,59–62]. Further investigation is still required to possibly confirm the presence of labile/nonspecific protein interactions and provide a better perspective in establishing a quantitative link between the molecular interplay at the microscopic scale and the biophysical properties of BP. Progress in these directions will narrow even more the gap in understanding between the biology and rheology of the biofluid.

IV. CONCLUSIONS

We have experimentally quantified the linear viscoelasticity of blood plasma (BP) by determining its frequency-dependent complex shear modulus G^*. Human plasma samples collected from three donors were probed using multiple particle tracking microrheology and the steady shear rheology of the biofluid—which revealed a mild shear-thinning—was obtained using a rotational rheometer. Plasma proteins (namely, albumin, fibrinogen, and immunoglobulins G and M) were separately dissolved at physiological concentrations in a phosphate-buffered saline (pH 7.4) and probed as well, in order to investigate their contribution to the bulk rheology. The corresponding mean-squared displacements (MSDs) of the embedded colloids revealed no evidence of non-Fickian diffusion within the frequency range probed, i.e., MSD $\propto \tau$ for all lag times (Newtonian behavior). The proteins were then mixed together at physiological concentrations in the same buffer solution; a mixture of immunoglobulins (G, M, and A) was equally prepared. Like in BP, the MSDs obtained for the physiologically relevant analog protein solutions—i.e., model BP—exhibited logarithmic slopes lower than unity at short timescales and inferred frequency responses reminiscent of a Jeffreys fluid. The viscosity η_0 of all the fluids was extracted from the purely viscous long-time slope (zero-shear limit) of the MSDs, appearing to be dependent mainly on protein concentration. In conclusion, we put forth the combined effects of protein concentration, molecular weight, and/or extensibility as the cause for the weakly elastic behavior observed in shear.

Notably, the results presented also provide insight into the complex rheology of whole blood, whose elastic stress response begins at the molecular level via protein relaxation and protein-driven red blood cell aggregation [8].

ACKNOWLEDGMENTS

The authors thank Professor K. M. Schultz for helpful discussions, Dr. J. P. Leite for the protein solutions preparation and the Biointerfaces and Nanotechnology i3S scientific platform for the support. This material is based upon work supported by FEDER (COMPETE 2020), FCT/MCTES (PIDDAC) and FCT under Grants Nos. PTDC/EME-EME/30764/2017, PTDC/EME-APL/3805/2021, PTDC/QUI-QFI/29914/2017, 2021.06532.BD, UIDB/00532/2020, UIDP/00532/2020 and LA/P/0045/2020.

AUTHOR DECLARATIONS

Conflict of Interest

The authors have no conflicts to disclose.

REFERENCES

[1] Horner, J. S., M. J. Armstrong, N. J. Wagner, and A. N. Beris, "Measurements of human blood viscoelasticity and thixotropy under steady and transient shear and constitutive modeling thereof," J. Rheol. **63**, 799–813 (2019).

[2] Sousa, P. C., R. Vaz, A. Cerejo, M. S. N. Oliveira, M. A. Alves, and F. T. Pinho, "Rheological behaviour of human blood in uniaxial extensional flow," J. Rheol. **62**, 447–456 (2018).

[3] Armstrong, M., and J. Tussing, "A methodology for adding thixotropy to Oldroyd-8 family of viscoelastic models for characterization of human blood," Phys. Fluids **32**, 094111 (2020).

[4] Rodrigues, T., F. J. Galindo-Rosales, and L. Campo-Deaño, "Haemodynamics around confined microscopic cylinders," J. Non-Newton. Fluid Mech. **286**, 104406 (2020).

[5] Brust, M., C. Schaefer, R. Doerr, L. Pan, M. Garcia, P. E. Arratia, and C. Wagner, "Rheology of human blood plasma: Viscoelastic versus Newtonian behavior," Phys. Rev. Lett. **110**, 078305 (2013).

[6] Boron, W. F., and E. L. Boulpaep, *Medical Physiology: A Cellular and Molecular Approach*, 2nd ed. (Saunders, Philadelphia, 2012).

[7] Hall, J. E., *Guyton and Hall Textbook of Medical Physiology*, 13th ed. (Elsevier, Philadelphia, 2016).

[8] Brust, M., O. Aouane, M. Thiébaud, D. Flormann, C. Verdier, L. Kaestner, M. W. Laschke, H. Selmi, A. Benyoussel, T. Podgorski, G. Coupier, C. Misbah, and C. Wagner, "The plasma protein fibrinogen stabilizes clusters of red blood cells in microcapillary flows," Sci. Rep. **4**, 4348 (2014).

[9] Varchanis, S., Y. Dimakopoulos, C. Wagner, and J. Tsamopoulos, "How viscoelastic is human blood plasma?," Soft Matter **14**, 4238–4251 (2018).

[10] Mitra, H., P. Jayaram, A. Bratsman, T. Gabel, and K. Alba, "Characterization and rheology of platelet-rich plasma," J. Rheol. **64**, 1017–1034 (2020).

[11] Windberger, U., P. Baroni, and L. Noirez, "Capillary-size flow of human blood plasma: Revealing hidden elasticity and scale dependence," J. Biomed. Mater. Res. A **110**, 298–303 (2022).

[12] Kundukad, B., and J. R. C. van der Maarel, "Control of the flow properties of DNA by topoisomerase II and its targeting inhibitor," Biophys. J. **99**, 1906–1915 (2010).

[13] Jay, G. D., J. R. Torres, M. L. Warman, M. C. Laderer, and K. S. Breuer, "The role of lubricin in the mechanical behaviour of synovial fluid," Proc. Natl. Acad. Sci. U.S.A. **104**, 6194–6199 (2007).

[14] Huck, B. C., O. Hartwig, A. Biehl, K. Schwarzkopf, C. Wagner, B. Loretz, X. Murgia, and C.-M. Lehr, "Macro- and microrheological

properties of mucus surrogates in comparison to native intestinal and pulmonary mucus," Biomacromolecules **20**, 3504–3512 (2019).
[15] Jawerth, L., E. Fischer-Friedrich, S. Saha, J. Wang, T. Franzmann, X. Zhang, J. Sachweh, M. Ruer, M. Ijavi, S. Saha, J. Mahamid, A. A. Hyman, and F. Jülicher, "Protein condensates as aging Maxwell fluids," Science **370**, 1317–1323 (2020).
[16] Pan, W., L. Filobelo, N. D. Q. Pham, O. Galkin, V. V. Uzunova, and P. G. Vekilov, "Viscoelasticity in homogeneous protein solutions," Phys. Rev. Lett. **102**, 058101 (2009).
[17] Elbaum-Garfinkle, S., Y. Kim, K. Szczepaniak, C. C.-H. Chen, C. R. Eckmann, S. Myong, and C. P. Brangwynne, "The disordered P granule protein LAF-1 drives phase separation into droplets with tunable viscosity and dynamics," Proc. Natl. Acad. Sci. U.S.A. **112**, 7189–7194 (2015).
[18] Bergman, M. J., T. Garting, P. Schurtenberger, and A. Stradner, "Experimental evidence for a cluster glass transition in concentrated lysozyme solutions," J. Phys. Chem. B **123**, 2432–2438 (2019).
[19] Yang, D., M. Daviran, K. M. Schultz, and L. M. Walker, "Droplet-based microfluidic tool to quantify viscosity of concentrating protein solutions," Pharm. Res. **38**, 1765–1775 (2021).
[20] Bujacz, A., "Structures of bovine, equine and leporine serum albumin," Acta Cryst. D **68**, 1278–1289 (2012).
[21] Saphire, E. O., P. W. H. I. Parren, R. Pantophlet, M. B. Zwick, G. M. Morris, P. M. Rudd, R. A. Dwek, R. L. Stanfield, D. R. Burton, and I. A. Wilson, "Crystal structure of a neutralizing human IgG against HIV-1: A template for vaccine design," Science **293**, 1155–1159 (2001).
[22] Kollman, J. M., L. Pandi, M. R. Sawaya, M. Riley, and R. F. Doolittle, "Crystal structure of human fibrinogen," Biochemistry **48**, 3877–3886 (2009).
[23] Perkins, S. J., A. S. Nealis, B. J. Sutton, and A. Feinstein, "Solution structure of human and mouse immunoglobulin M by synchrotron X-ray scattering and molecular graphics modelling: A possible mechanism for complement activation," J. Mol. Biol. **221**, 1345–1366 (1991).
[24] Waigh, T. A., "Microrheology of complex fluids," Rep. Prog. Phys. **68**, 685–742 (2005).
[25] Mason, T. G., and D. A. Weitz, "Optical measurements of frequency-dependent linear viscoelastic moduli of complex fluids," Phys. Rev. Lett. **74**, 1250–1253 (1995).
[26] Mason, T. G., "Estimating the viscoelastic moduli of complex fluids using the generalized Stokes–Einstein equation," Rheol. Acta **39**, 371–378 (2000).
[27] Dasgupta, B. R., S.-Y. Tee, J. C. Crocker, B. J. Frisken, and D. A. Weitz, "Microrheology of polyethylene oxide using diffusing wave spectroscopy and single scattering," Phys. Rev. E **65**, 051505 (2002).
[28] Wehrman, M. D., S. Lindberg, and K. M. Schultz, "Multiple particle tracking microrheology measured using bi-disperse probe diameters," Soft Matter **14**, 5811–5820 (2018).
[29] Lu, Q., and M. J. Solomon, "Probe size effects on the microrheology of associating polymer solutions," Phys. Rev. E **66**, 061504 (2002).
[30] Chen, D. T., E. R. Weeks, J. C. Crocker, M. F. Islam, R. Verma, J. Gruber, A. J. Levine, T. C. Lubensky, and A. G. Yodh, "Rheological microscopy: Local mechanical properties from microrheology," Phys. Rev. Lett. **90**, 108301 (2005).
[31] See the supplementary material at https://www.scitation.org/doi/suppl/10.1122/8.0000442 for additional information regarding particle tracking errors (Sec. S1), hydrodynamic interactions with the sample chamber walls (Sec. S2) and validation of our experimental setup (Sec. S3).
[32] Crocker, J. C., and D. G. Grier, "Methods of digital video microscopy for colloidal studies," J. Colloid Interface Sci. **179**, 298–310 (1996).
[33] Savin, T., and P. S. Doyle, "Static and dynamic errors in particle tracking microrheology," Biophys. J. **88**, 623–638 (2005).
[34] Schultz, K. M., and E. M. Furst, "Microrheology of biomaterial hydrogelators," Soft Matter **8**, 6198–6205 (2012).
[35] Ewoldt, R. H., M. T. Johnston, and L. M. Caretta, "Experimental challenges of shear rheology: How to avoid bad data," in *Complex Fluids in Biological Systems*, edited by S. E. Spagnolie (Springer, New York, NY, 2015), pp. 207–241.
[36] Reif, F., *Fundamentals of Statistical and Thermal Physics* (Waveland Press, Long Grove, IL, 1965).
[37] Raikher, Y. L., V. V. Rusakov, and R. Perzynski, "Brownian motion in a viscoelastic medium modelled by a Jeffreys fluid," Soft Matter **9**, 10857–10865 (2013).
[38] Grimm, M., S. Jeney, and T. Franosch, "Brownian motion in a Maxwell fluid," Soft Matter **7**, 2076–2084 (2011).
[39] Makris, N., and G. Kampas, "Analyticity and causality of the three-parameter rheological models," Rheol. Acta **48**, 815–825 (2009).
[40] Savin, T., and P. S. Doyle, "Statistical and sampling issues when using multiple particle tracking," Phys. Rev. E **76**, 021501 (2007).
[41] Rich, J. P., G. H. McKinley, and P. S. Doyle, "Size dependence of microprobe dynamics during gelation of a discotic coloidal clay," J. Rheol. **55**, 273–299 (2011).
[42] Crocker, J. C., M. T. Valentine, E. R. Weeks, T. Gisler, P. D. Kaplan, A. G. Yodh, and D. A. Weitz, "Two-point microrheology of inhomogeneous soft materials," Phys. Rev. Lett. **85**, 888–891 (2000).
[43] McGlynn, J. A., N. Wu, and K. M. Schultz, "Multiple particle tracking microrheological characterization: Fundamentals, emerging techniques and applications," J. Appl. Phys. **127**, 201101 (2020).
[44] Berg, H. C., *Random Walks in Biology*, 2nd ed. (Princeton University Press, Princeton, NJ, 1993).
[45] Bird, R. B., R. C. Armstrong, and O. Hassager, *Dynamics of Polymeric Liquids, Volume 1: Fluid Mechanics*, 2nd ed. (Wiley, New York, NY, 1987).
[46] Ferry, J. D., *Viscoelastic Properties of Polymers*, 3rd ed. (Wiley, New York, NY, 1980).
[47] Balogun, A., D. Lazarenko, F. Khabaz, and R. Khare, "Extending the timescale of molecular simulations by using time–temperature superposition: Rheology of ionic liquids," Soft Matter **17**, 7210–7220 (2021).
[48] Cox, W. P., and E. H. Merz, "Correlation of dynamic and steady flow viscosities," J. Polym. Sci. **28**, 619–622 (1958).
[49] Castellanos, M. M., J. A. Pathak, and R. H. Colby, "Both protein adsorption and aggregation contribute to shear yielding and viscosity increase in protein solutions," Soft Matter **10**, 122–131 (2014).
[50] Gudapati, H., D. Parisi, R. H. Colby, and I. T. Ozbolat, "Rheological investigation of collagen, fibrinogen, and thrombin solutions for drop-on-demand 3D bioprinting," Soft Matter **16**, 10506–10517 (2020).
[51] Ariola, F. S., A. Krishnan, and E. A. Vogler, "Interfacial rheology of blood proteins adsorbed to the aqueous-buffer/air interface," Biomaterials **27**, 3404–3412 (2006).
[52] Zhang, Z., S. Barman, and G. F. Christopher, "The role of protein content on the steady and oscillatory shear rheology of model synovial fluids," Soft Matter **10**, 5965–5973 (2014).
[53] Chowdhury, A., G. Guruprasad, A. T. Chen, C. A. Karouta, M. A. Blanco, T. M. Truskett, and K. P. Johnston, "Protein-protein interactions, clustering, and rheology for bovine IgG up to high concentrations characterized by small angle X-ray scattering and molecular dynamics simulations," J. Pharm. Sci. **109**, 696–708 (2020).
[54] Bekard, I. B., P. Asimakis, J. Bertolini, and D. E. Dunstan, "The effects of shear flow on protein structure and function," Biopolymers **95**, 733–745 (2011).

[55] Lauser, K. T., A. L. Rueter, and A. Calabrese, "Small-volume extensional rheology of concentrated protein and protein excipient solutions," Soft Matter **17**, 9624–9635 (2021).

[56] Hämisch, B., A. Büngeler, C. Kielar, A. Keller, O. Strube, and K. Huber, "Self-assembly of fibrinogen in aqueous, thrombin-free solutions of variable ionic strengths," Langmuir **35**, 12113–12122 (2019).

[57] Martin-Alarcon, L., and T. A. Schmidt, "Rheological effects of macromolecular interactions in synovial fluid," Biorheology **53**, 49–67 (2016).

[58] Haward, S. J., "Synovial fluid response to extensional flow: Effects of dilution and intermolecular interactions," PLoS One **9**, e92867 (2014).

[59] Eilat, D., R. Fischel, and A. Zlotnick, "Albumin–immunoglobulin complexes in human serum: Classification and immunochemical analysis," Scand. J. Immunol. **14**, 77–87 (1981).

[60] Koopman, J., F. Haverkate, J. Grimbergen, L. Engesser, I. Nováková, A. F. J. A. Kerst, and S. T. Lord, "Abnormal fibrinogens IJmuiden (BβArg$_{14}$→Cys) and Nijmegen (BβArg$_{44}$→Cys) form disulfide-linked fibrinogen–albumin complexes," Proc. Natl. Acad. Sci. U.S.A. **89**, 3478–3482 (1992).

[61] Lipinski, B., and E. M. Sajdel-Sulkowska, "New insight into Alzheimer disease: Demonstration of fibrin(ogen)-serum albumin insoluble deposits in brain tissue," Alzheimer Dis. Assoc. Disord. **20**, 323–326 (2006).

[62] Sauls, D. L., M. Warren, and M. Hoffman, "Homocysteinylated fibrinogen forms disulfide-linked complexes with albumin," Thromb. Res. **127**, 576–581 (2011).

[63] Campo-Deaño, L., R. P. A. Dullens, D. G. A. L. Aarts, F. T. Pinho, and M. S. N. Oliveira, "Viscoelasticity of blood and viscoelastic blood analogues for use in polydymethylsiloxane *in vitro* models of the circulatory system," Biomicrofluidics **7**, 034102 (2013).